Role of Si clusters in the phase transformation and formation of (6×6)-ring structures on 6H-SiC(0001) as a function of temperature: An STM and XPS study

W. J. Ong[1,2] and E. S. Tok[1,2,*]
[1]*Department of Physics, National University of Singapore, Kent Ridge, Singapore 119260, Singapore*
[2]*Institute of Materials Research and Engineering, IMRE Building, 3 Research Link, Singapore 117602, Singapore*
(Received 17 May 2005; revised manuscript received 3 November 2005; published 30 January 2006)

We report the formation of the 6H-SiC(0001)/(6×6) ring structure using scanning tunneling microscopy (STM) and x-ray photoemission spectroscopy. This reconstruction is obtained from the evolution of surface structures with progressive annealing; starting from a (3×3) phase at 850 °C→Si rich (6×6) clusters at 1000 °C→(6×6) rings at 1100 °C. We show that this ring structure can be described by a (6×6) unit cell rather than a $(6\sqrt{3}\times 6\sqrt{3})$ *R*30° reconstruction. STM evidence reveals the presence of type "A" clusters (size ~8 Å) and type "B" clusters (size ~14.3 Å) on the surface during this structural transformation. The density of these clusters decreases with progressive annealing, eventually leaving behind only the type "C" Si adatoms (size ~3 Å), which forms the ring structure at 1100 °C. This ring structure albeit less Si rich compared to the (6×6) cluster and the initial (3×3) surface is not graphitic. We propose a ball and stick model taking into consideration the role of Si as tetraclusters to describe the structural transformation and formation of the ring structure from the initial (3×3) reconstructed surface. We found that each structural phase observed can be accounted for by moving or removing at least $M\times 4$ Si atoms (where M=number of tetraclusters).

DOI: 10.1103/PhysRevB.73.045330 PACS number(s): 68.35.Bs, 68.47.Fg, 68.37.−d, 79.60.−i

I. INTRODUCTION

SiC is widely recognized as a substrate material for electronic device applications in areas where common silicon technology finds limitations. Unique properties such as a wide band gap, high thermal conductivity, high saturated electron drift velocity, and high breakdown field strength have generated microelectronic applications in high-temperature as well as chemically hostile environments especially in high-voltage, high-frequency, and high-power applications.[1] In particular, the current push for continuing device miniaturization has led to great interest in nanostructure formation on SiC surfaces. While SiC exists in various polytypes depending on the bulk atomic arrangement,[2] much of the recent work has been focused on the 6H-SiC(0001) which exhibits several surface reconstructions ranging from (3×3), $(\sqrt{3}\times\sqrt{3})$, (5×5), $(2\sqrt{3}\times 2\sqrt{13})$, (6×6), and $(6\sqrt{3}\times 6\sqrt{3})R30°$ as shown by low-energy electron diffraction (LEED), reflection (high-energy electron diffraction, and scanning tunneling microscopy (STM) studies.[3–5,18,19] While the formation of these Si-rich reconstructions depends on the substrate temperature and the Si content on the surface, a graphitized surface occurs when the surface is heated beyond 1200 °C.[6]

The starting (3×3) reconstruction is easily the most studied structure and is currently most accurately described by the model proposed by Starke *et al.*[7–10] However, there is still much controversy surrounding the high-temperature surface phases of SiC(0001) when it is heated beyond 1000 °C, in particular, the $(6\sqrt{3}\times 6\sqrt{3})R30°$. Earlier diffraction studies have reported the existence of the $(6\sqrt{3}\times 6\sqrt{3})R30°$ surface structure upon heating to ~1200 °C,[11,12] which led some to propose that the structure could be due to an incommensurate graphite overlayer.[13,14] However, an x-ray photoemission spectroscopy (XPS) study of this surface by Johansson *et al.*[15] suggested that the $(6\sqrt{3}\times 6\sqrt{3})R30°$ reconstruction could be attributed to carbon in a Si-deficient environment and did not amount to surface graphitization. The graphitic surface only appeared after heating to temperatures greater than 1200 °C. It is important to note that despite exhaustive studies on this structure, there has been no real space STM evidence of the $(6\sqrt{3}\times 6\sqrt{3})R30°$ reconstruction to date. This was corroborated by Owman *et al.*, which studied the SiC surface heated at this temperature regime with STM.[16] They observed the coexistence of $(\sqrt{3}\times\sqrt{3})R30°$, (5×5), and (6×6) trimerlike reconstruction and did not detect any structure which exhibited $(6\sqrt{3}\times 6\sqrt{3})R30°$ periodicity. By comparing a Fourier analysis of the STM data with the LEED data, Owman *et al.* suggested that the $(6\sqrt{3}\times 6\sqrt{3})R30°$ pattern could be due to scattering from a surface with a mixture of $(\sqrt{3}\times\sqrt{3})R30°$, (5×5), and (6×6) trimerlike reconstructions. More recently, a high-temperature surface structure exhibiting a ringlike appearance was observed with STM when the substrate was heated to 1100 °C.[17,18] These ringlike structures were assigned as real STM images of the $(6\sqrt{3}\times 6\sqrt{3})R30°$ reconstruction,[17] which was in contrast to the observations by Owman *et al.* The reported measured ring separation of 2.5 nm, however, did not support a $(6\sqrt{3}\times 6\sqrt{3})R30°$ unit cell. Hence, despite the extensive study being done on the high temperature surface structures of 6H-SiC(0001), the elucidation of these structures is still elusive.

In our previous work, we have used STM to show that the initial (3×3) surface reconstruction undergoes disordering with the formation of type "A" (size ~8 Å) and "B" (size ~14.3 Å) clusters when the surface was heated from 850 to 950 °C. This was superceded by the self-assembly of type B clusters into an ordered (6×6) arrangement with no type A clusters detected at 1000 °C.[18,19] In an effort to resolve the surface structures observed at higher temperatures, we investigated the surface structural evolution further by

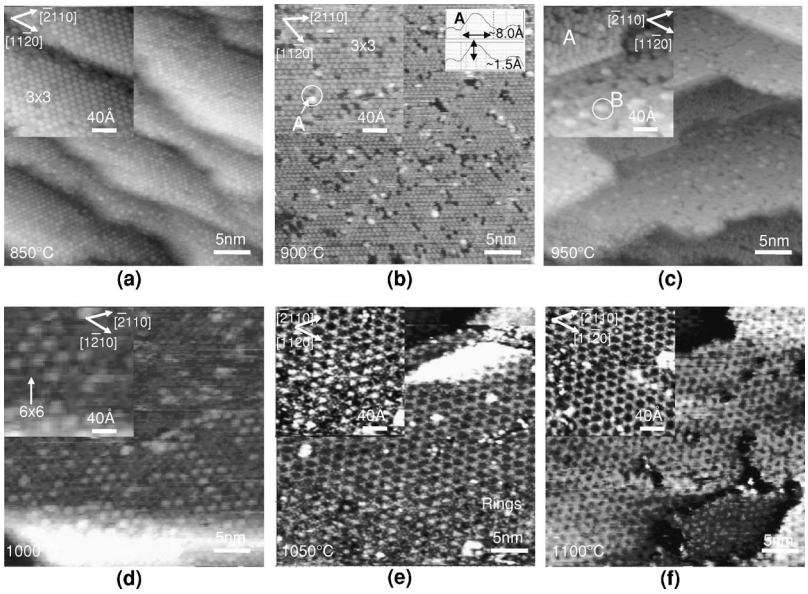

FIG. 1. A series of 40 nm×40 nm STM images of the surface morphology after annealing to temperatures of (a) 850 °C, (b) 900 °C, (c) 950 °C, (d) 1000 °C, (e) 1050 °C, and (f) 1100 °C. Corresponding inset images show high resolution 1.6 nm×1.6 nm STM pictures of (a) (3×3) reconstruction, (b) formation of type A from (3×3) and line profile of type A (average size ~8.0 Å, height ~1.5 Å), (c) coexistence of type A and B clusters, (d) self assembly of type B clusters into (6×6) superstructure, (e) absence of type B leaving only type A coexisting with rings, and (f) (6×6)-ringlike structures dominating surface structure.

heating this (6×6) cluster surface beyond 1000 °C. We will show the following in this work. (i) Disordering of the (6×6) cluster surface occurs with diminishing type B clusters density and the reemergence of type A clusters on the surface. The surface is eventually dominated by type C Si adatoms (size ~3.0 Å) which decorate the ring structure at 1100 °C. This structural evolution appears to occur with the loss of Si from the surface. (ii) By analyzing the unit cell dimensions, crystallographic azimuths and autocorrelation of the real space, we will show that this ring structure has a (6×6) and not $(6\sqrt{3}\times 6\sqrt{3})R30°$ unit cell. (iii) By incorporating the existence of Si as tetraclusters, we propose a ball and stick model to describe the structural transformation and the formation of the ring structure from the initial (3×3) reconstructed surface. We will show that each structural phase observed can be accounted by moving or removing at least $M\times 4$ Si atoms (where M=number of clusters).

II. EXPERIMENTAL

The experiments were carried *in situ* out in a UHV system with an OMICRON VT STM and a VG XPS, with an ambient pressure of 1.0×10^{-10} mbar. The samples were cut from *N*-doped *n*-type 6H-SiC(0001) single crystal wafers with dopant concentration of $\sim 10^{18}$ cm^{-3} supplied by CREE Research. The details of our sample preparation have been discussed previously.[18] Briefly, these samples were first chemically etched *ex situ* in 1:10 parts of 49% HF acid to deionized water before outgassing for 8 h at ~300 °C in the UHV chamber. Si was then deposited on the sample at room temperature followed by annealing at 850 °C. The sample was progressively annealed to 1200 °C in steps of 50 °C for 10 min before quenching down to room temperature. XPS and STM measurements were made immediately after each annealing step. The XPS spectra were recorded in constant pass energy mode of the analyzer using an Al $K\alpha$ x-ray source. The best fit curves were achieved after a Shirley-type background subtraction based on the same Lorentzian broadened by a Gaussian, in maintaining component peak shape and full widths at half maximum (FWHMs) using the standard manufacturer's software. All the STM images were taken using constant current mode, with tunneling currents of 0.05–1.00 nA and biases of up to ±4.0 V applied to the sample. The dimension and periodicity analysis were performed with the use of the WSXM software (Nanotec Electronica S.L. Sizes). The dimensions of the clusters and ring structures were derived as an average of the cross-sectional diameter and depth, respectively. These values were measured with the line profile software in the [1010], [1210], and [2110] crystallographic directions, as described in our previous paper.[18]

III. RESULTS AND DISCUSSION

A. Global phase transformation: (3×3)→(6×6) clusters →ring structure

Figures 1(a)–1(f) show the STM images (40 nm ×40 nm) of the surface after annealing the 6H-SiC(0001) substrate to temperatures of 850, 900, 950, 1000, 1050, and 1100 °C, respectively. The inset images are higher resolution images of the corresponding surface obtained at a scan size of 16 nm×16 nm.

By annealing the substrate to a temperature of 850 °C, we obtain the initial (3×3) surface structure [Fig. 1(a)]. At higher temperatures, a (6×6) cluster superstructure is obtained at 1000 °C [Fig. 1(d)], while formation of ringlike structures over wide terraces occurs at 1100 °C [Fig. 1(f)]. In the temperature regime going from (3×3) [Fig. 1(a)] to the (6×6) clusters phase [i.e., Fig. 1(c)], occurrence of two types of clusters with an average size of ~8.0±0.5 Å and ~14.3±0.5 Å, as well as an average height of ~1.5±0.5 Å and ~2.3±0.5 Å are also observed on the surface. We have previously labeled these clusters as type A and type B clusters, respectively.[18] A more interesting observation, however, is the appearance of similar cluster features in shape and size respective to the type A and B clusters when the surface

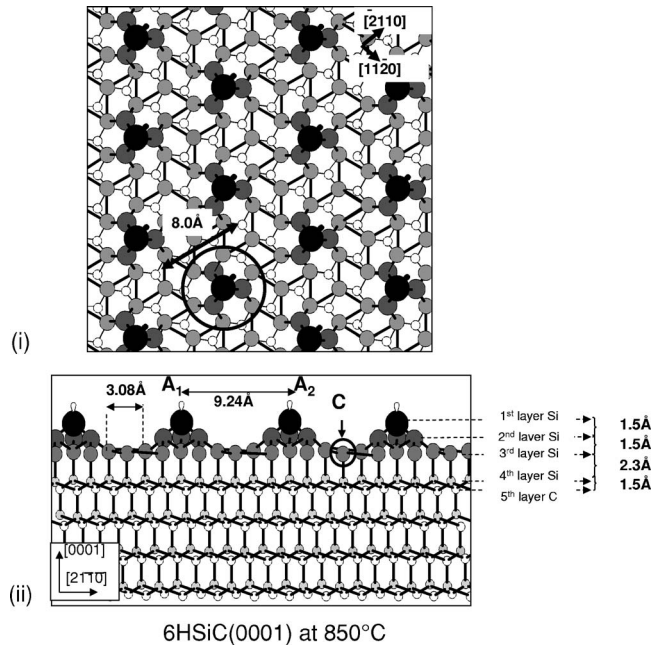

FIG. 2. A schematic (i) plan view and (ii) side view of the (3×3) reconstruction formed at 850 °C proposed by Starke *et al.* (Refs. 7–10).

transforms from the (6×6) cluster phase at 1000 °C to a disordered phase at 1050 °C [Fig. 1(e)] and later in the formation of ring structures with a depression at the center at 1100 °C [Fig. 1(f)].

It is evident from Fig. 1 that as the annealing temperature increases, the STM images reveal a significant atomic rearrangement of the initial (3×3) surface structure. According to Starke's model,[7–10] this (3×3) reconstruction is a structure consisting of Si atoms existing as tetrahedral clusters arranged along the $[11\bar{2}0]$ and $[\bar{2}110]$ azimuths. These Si tetraclusters are described as having one Si adatom sitting above a Si trimer structure in the second layer, which are in turn arranged above a full Si adlayer existing on top of the Si-terminated SiC bulk. This configuration of Si atoms makes up the first four layers of substrate and accounts for the (3×3) reconstruction being described as a Si-rich structure. As this structure will form the basis for our discussion in the later section, it is reproduced as shown in Fig. 2 as a ball and stick model and in both plane and side views.

By comparing the density of atoms on the surface of the (3×3) reconstruction prepared at 850 °C with the final ring structure obtained at 1100 °C, as shown in Fig. 1, the surface has clearly changed from a compact and high density Si-rich structure to a surface that is decorated with depressions/vacancies. This morphological changes clearly indicate a loss of material and it occurs probably through desorption of Si when the substrate is progressively heated to 1100 from 850 °C. Apart from STM data, evidence for the loss material as Si can also be inferred from the XPS measurements (Figs. 3 and 4) corresponding to the surfaces shown in Fig. 1.

Figure 3(a) shows the best fit XPS spectra for the Si $2p$ signal after chemical etching and outgassing in UHV (as received), after Si deposition at room temperature and after annealing to temperatures ranging from 800 to 1200 °C. In the Si $2p$ core level spectrum, we can distinguish two contributions at binding energy of 99.3 and 102.0 eV. The component at 102.0 eV is detected from the surface after chemical etching and is attributed to the Si-C bonding in the SiC bulk. The component at 99.3 eV only appears upon Si deposition at room temperature and is due to Si-Si bonding de-

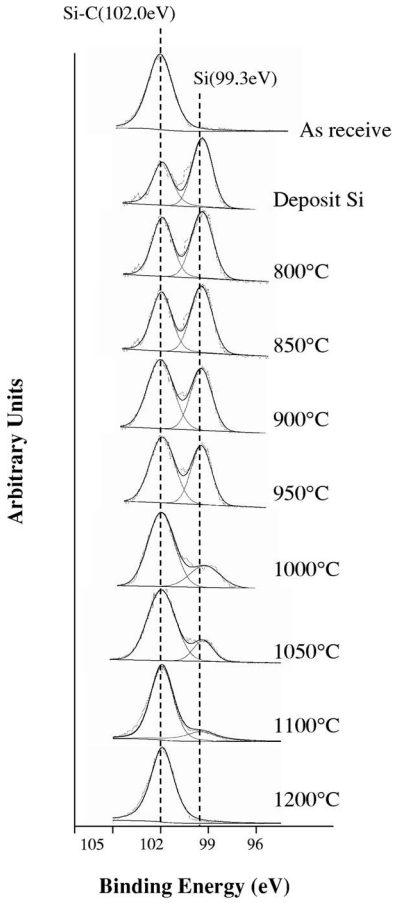

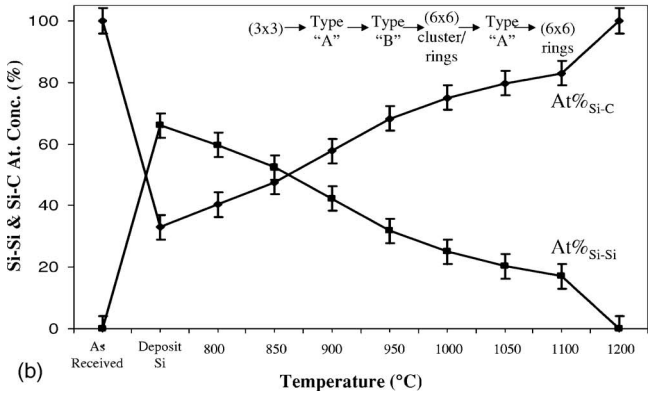

FIG. 3. (a) The peak fitted Si $2p$ signal (i.e., elemental Si component at 99.3 eV and the Si-C component at 103.0 eV) due to surface after chemical etch, after Si deposition at room temperature and after annealing the substrate to different temperatures. (b) Relative atomic concentration percent of Si-Si and Si-C as a function of annealing temperature. Note that the XPS peak area intensity for the (3×3) structure (850 °C) and (6×6) ring structure (1100 °C) is 726 and 236 counts, respectively.

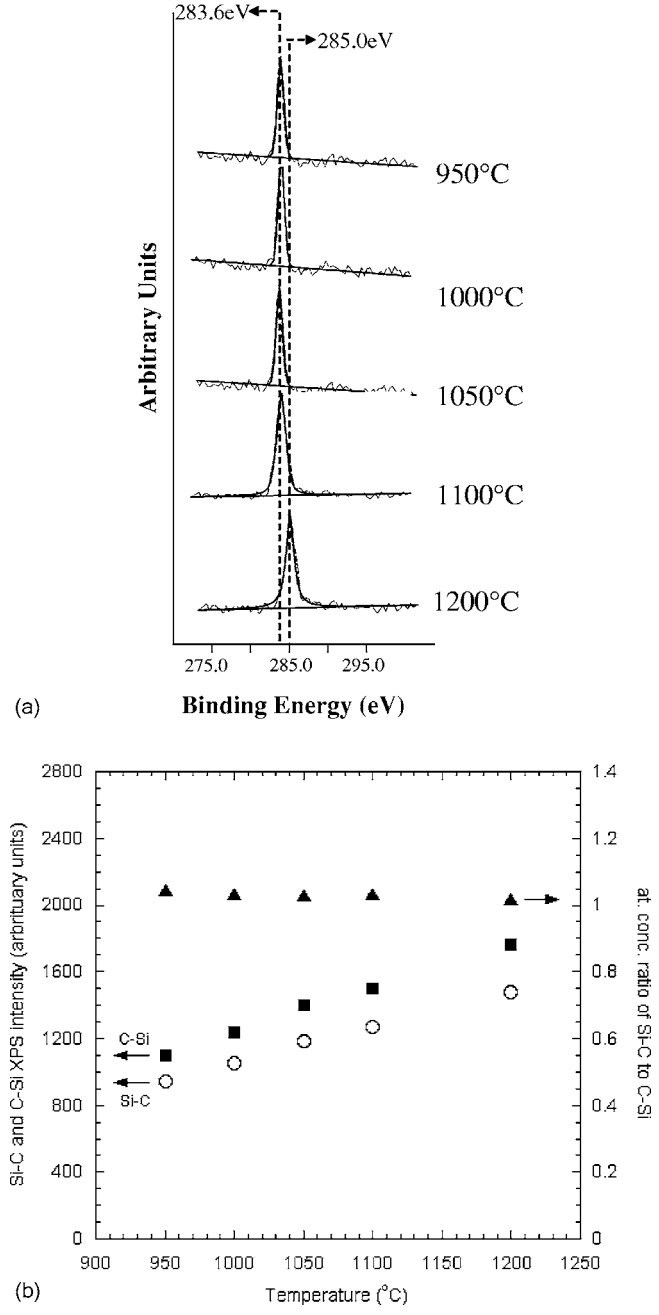

FIG. 4. (a) The peak fitted C 1*s* signal (283.6 eV) at various annealing temperatures. The C 1*s* peak binding energy is observed to shift to 285.0 eV at 1200 °C. (b) The intensities of C-Si and Si-C as well as the Si-C:C-Si atomic concentration ratio, as a function of annealing temperature.

rived from the presence of elemental Si now present at the surface.[18]

In order to extract information about the surface Si stoichiometry corresponding to the various surface reconstructions arising from progressive annealing, we compare the relative atomic concentration of Si-C (at. $\%_{\text{Si-C}}$) and Si-Si (at. $\%_{\text{Si-Si}}$) as shown in Fig. 3(b), obtained from the following expressions:

$$\text{at. }\%_{\text{Si-Si}} = \left[\frac{\dfrac{I_{\text{Si-Si}}}{(\text{ASF})_{\text{Si }2p} \times \text{TF}}}{\dfrac{I_{\text{Si-Si}}}{(\text{ASF})_{\text{Si }2p} \times \text{TF}} + \dfrac{I_{\text{Si-C}}}{(\text{ASF})_{\text{Si }2p} \times \text{TF}}} \right] \times 100\,\%\,,$$

$$\text{at. }\%_{\text{Si-C}} = \left[\frac{\dfrac{I_{\text{Si-C}}}{(\text{ASF})_{\text{Si }2p} \times \text{TF}}}{\dfrac{I_{\text{Si-Si}}}{(\text{ASF})_{\text{Si }2p} \times \text{TF}} + \dfrac{I_{\text{Si-C}}}{(\text{ASF})_{\text{Si }2p} \times \text{TF}}} \right] \times 100\,\%\,,$$

where I is the peak intensity (total area under curve fitted peak), ASF is the atomic sensitivity factor for Si 2*p*, and TF is the spectrometer transmission function.

From Fig. 3(b), the at. $\%_{\text{Si-Si}}$ and at. $\%_{\text{Si-C}}$ associated with the (3×3) at 850 °C is shown to be 52.4 and 47.6%, respectively. Further annealing to higher temperatures shows that at. $\%_{\text{Si-Si}}$ follows a decreasing trend with respect to an increasing at. $\%_{\text{Si-C}}$. In particular, the ring structure formed at 1100 °C is found to have at. $\%_{\text{Si-Si}}$ of 17.0% and at. $\%_{\text{Si-C}}$ of 83%. The presence of elemental Si (at. $\%_{\text{Si-Si}} \sim 17.0\%$) indicates that the ring structure is still slightly Si rich.

Figure 4(a) shows the curve fitted C 1*s* spectra as the surface was annealed from 950 to 1200 °C. Figure 4(b) shows the peak area intensities due to C in a SiC environment ($I_{\text{C-Si}}$) and Si in a SiC environment ($I_{\text{C-Si}}$) derived from both Figs. 3(a) and 4(a). The corresponding atomic concentration for C-Si (at. $\%_{\text{C-Si}}$) and Si-C (at. $\%_{\text{Si-C}}$) are also presented in Fig. 4(b) and were obtained from the following expressions:

$$\text{at. }\%_{\text{C-Si}} = \left[\frac{\dfrac{I_{\text{C-Si}}}{(\text{ASF})_{\text{C}1s} \times \text{TF}}}{\dfrac{I_{\text{C-Si}}}{(\text{ASF})_{\text{C}1s} \times \text{TF}} + \dfrac{I_{\text{Si-C}}}{(\text{ASF})_{\text{Si }2p} \times \text{TF}}} \right] \times 100\,\%\,,$$

$$\text{at. }\%_{\text{Si-C}} = \left[\frac{\dfrac{I_{\text{Si-C}}}{(\text{ASF})_{\text{Si }2p} \times \text{TF}}}{\dfrac{I_{\text{C-Si}}}{(\text{ASF})_{\text{C}1s} \times \text{TF}} + \dfrac{I_{\text{Si-C}}}{(\text{ASF})_{\text{Si }2p} \times \text{TF}}} \right] \times 100\,\%\,,$$

while both the intensities of C-Si and Si-C increase with temperature, however, the ratio of C-Si atomic concentration to Si-C atomic concentration (i.e., C-Si:Si-C) remains constant at approximately 1.0 with a deviation of $<3\%$ at each annealing temperature. Since the bulk stoichiometry is clearly maintained, the increase in both the intensities can be attributed to an increased exposure of the SiC bulk.

These observations suggest a loss of elemental Si from the surface. Since the initial (3×3) surface is composed of four layers of covalently bonded Si atoms, the progressive reduction in the elemental Si at higher temperatures could be attributed to the loss of Si from the surface. This could occur through the breaking of Si-Si bonds within these layers and release of Si from the surface as a consequence. The increase in the loss of these Si atoms with increasing temperature would inevitably lead to a greater exposure of the underlying

Si-C layers, which would account for the greater Si-C bonding presence at the surface of the SiC substrate. A more intense Si 2*p* peak or C-1*s* peak associated with the Si-C bonding would thus be observed with progressive annealing.

Additional analysis of the Si-C related C 1*s* peak detected at a binding energy of 283.6 eV shows that there is no shift in the binding energy of the C 1*s* peak even after annealing the surface to 1100 °C. In fact, the XPS data [Fig. 3(b)] still reveals the presence of a weak elemental Si signal at 99.3 eV. The ring structure observed at 1100 °C is therefore still slightly Si rich. In fact this Si peak at 99.3 eV only disappears upon heating to 1200 °C. When this happens, a shift in the C 1*s* peak from 283.6 to 285.0 eV also occurs. These observations would suggest a formation of a carbon rich surface and the C 1*s* binding energy detected at 285.0 eV is also indicative of the formation of C-C bonds.[15]Although not this is not the main focus of the present work, STM studies performed by others at this particularly high temperature reveals the formation of a graphitic surface on the SiC substrate instead.[6,13–15]

The current XPS study therefore shows that the ring structures observed at 1100 °C are neither a carbon rich nor a graphitic surface. The formation of the ring structures at 1100 °C still exists in the Si-rich regime albeit much less than the initial (3×3) and also (6×6) cluster phase. More significantly, the phase transformation leading to the ring structures from (3×3) appears to proceed with Si-Si bond breaking resulting in Si loss from the surface. The formation of various surface reconstructions arising from Si evaporation has also been reported for other SiC substrate surfaces such as the cubic SiC(001) surface.[21] Unlike this previous work, we have also noted the trend of Si clusters formation coexisting with depressions [see Figs. 1(b), 1(c), and 1(e)] on the surface accompanying the structural transition.

With the aid of high-resolution STM, we will study this surface evolution in greater detail. In particular, we will focus on the role of Si clusters leading to the formation of the ring structures from the (6×6) cluster phase beginning with the initial (3×3) surface prepared at 850 °C.

B. Si clusters and phase transformation: $(3\times3)\rightarrow(6\times6)$ clusters$\rightarrow(6\times6)$ ring structures

1. $(3\times3)\rightarrow(6\times6)$ *clusters*

The surface evolution from a (3×3) surface to a (6×6)-cluster surface has been described in detail in Ref. 18. Thus only key points of this structural transformation and the corresponding mechanism will be discussed. This is necessary in order to formulate an understanding of this phase transformation involving Si clusters in the later sections.

The inset of Fig. 1(a) is a high-resolution scan showing a well ordered surface after annealing at 850 °C, consisting of bright protrusions aligned along the $[11\bar{2}0]$ and $[\bar{2}110]$ crystallographic azimuths. The separation between each adjacent bright protrusion measured along both azimuths is ~9.0 Å. This periodic arrangement is three times the SiC(0001)-(1×1) unit cell (lattice parameter=3.08 Å), giving rise to a reconstruction with a (3×3) unit cell.

As shown in Fig. 2, these Si tetraclusters are arranged above a full Si adlayer in the third layer of the structure, which are in turn held by the fourth Si layer terminating the bulk SiC. Also shown in Fig. 2 is the separation of each Si layer in the [0001] azimuth. Hence, the (3×3) reconstruction as shown in Fig. 1(a) (inset) would consist of one tetracluster per unit cell. All the Si atoms are fourfold coordinated except for the top Si adatom in the tetracluster, which has a single dangling bond. The bright protrusions observed in empty state imaging on the (3×3) surface is therefore attributed to electrons tunneling into the empty states associated with the single dangling bond on each of the top Si adatom. The plane view of the Starke model illustrated in Fig. 2(a) shows the structure drawn with the Si-adlayer atoms occupying bulk SiC positions and the Si atoms within the tetracluster having a Si-Si bond length of ~2.3 Å.[12] In this structural configuration, the Si tetracluster would have a diameter of 8.0±0.5 Å and a height of 1.5±0.2 Å. Hence the spatial area occupied by a tetracluster from the model in plane view is akin to the size of the electron cloud attributed to one tetracluster observed by STM as shown in Fig. 1(b) (inset line profile) (i.e., average size ~8.0±0.5 Å, height ~1.5±0.5 Å).

The high-resolution inset image of the surface after annealing at 900 °C is shown in Fig. 1(b). A disordered phase is now observed to coexist with the ordered (3×3) reconstruction These disordered domains consist of round clusters and neighboring vacancies, which show up as bright and dark features, respectively. They are real physical features and are not electronic effects, as STM biasing does not reveal any changes to the feature sizes observed. STM line profile analysis of both types of features show that they each possess an average size and height (depth) of ~8.0±0.5 Å (9.0±0.5 Å) and 1.5±0.5 Å (2.0±0.5 Å) for clusters (for vacancies), respectively. These bright features have been previously identified as type A clusters[18] and appear similar in shape and size to a (3×3) tetracluster. Hence the formation of type A clusters and vacancies of similar size imply a consequence of tetraclusters being released from the (3×3) surface, which is schematically illustrated in Fig. 5(a).

At 950 °C [Fig. 1(c)], the (3×3) reconstruction is no longer observed. Instead, the surface structure is now dominated by more disordered type A clusters and larger round-like type B clusters which are measured to be ~14.3±0.5 Å (size) and 2.3±0.5 Å (height). Further annealing to 1000 °C as shown in Fig. 1(d), shows no trace of type A clusters but the existence of only type B clusters which appear to be organized into an ordered hexagonal (6×6) periodic arrangement in the $[11\bar{2}0]$ and $[\bar{2}110]$ azimuths.

The STM evidence suggests that type A clusters occur through the release of individual tetraclusters from (3×3) reconstruction, hence the formation of type B clusters could proceed via agglomeration of a few type A clusters. Figure 5(b) illustrates schematically the agglomeration of type A clusters to form the new type B feature. The ordering of the type B clusters resulting in (6×6) periodicity along the $[11\bar{2}0]$ and $[\bar{2}110]$ azimuths is shown in schematically in Fig. 5(c). Superimposed onto Fig. 5(b) is a dotted circle representing the actual measured diameter of a B cluster

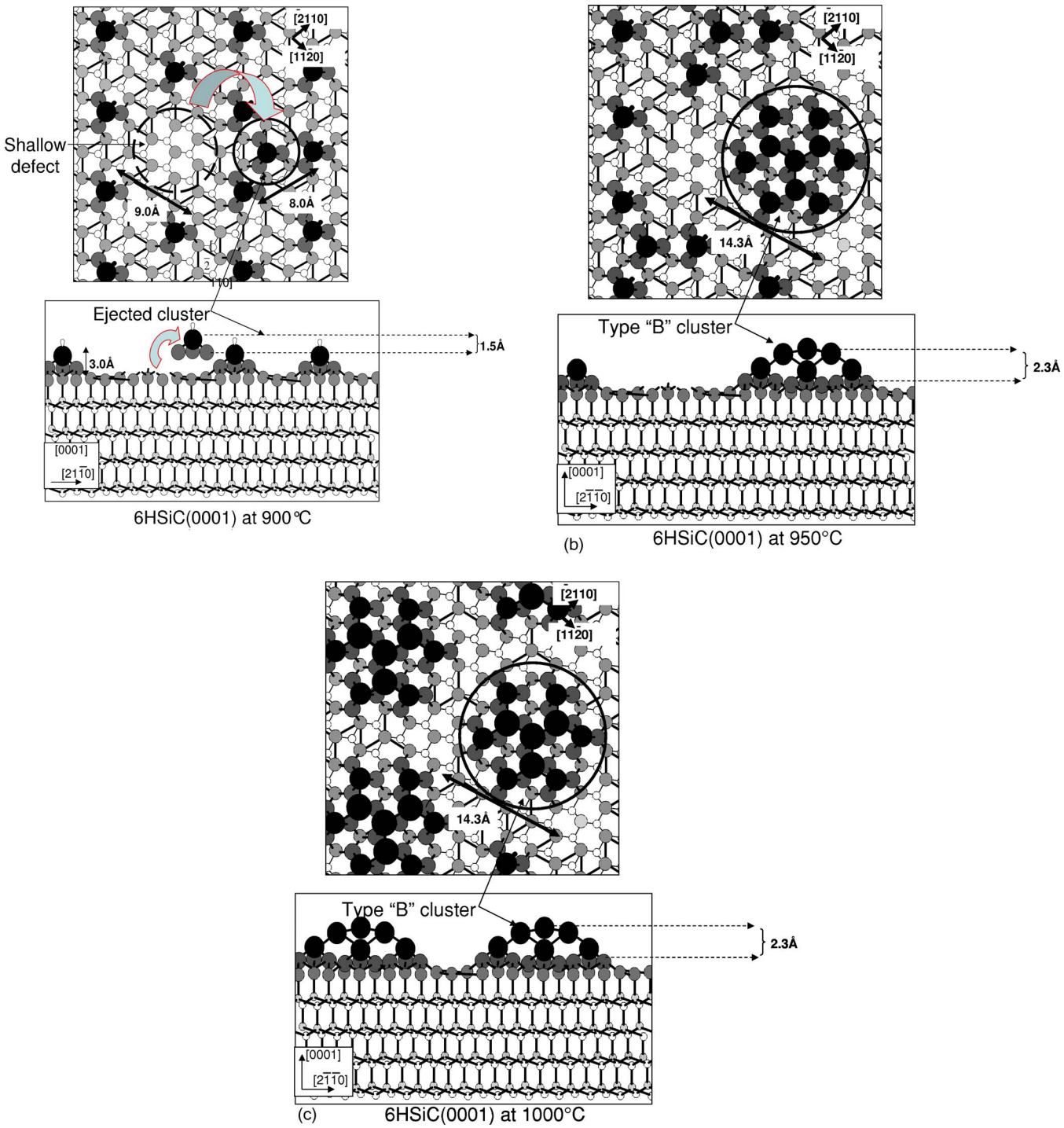

FIG. 5. (Color online) (a) The ejection of a tetracluster (size ~8.0 Å height ~1.5 Å) from the (3×3) reconstructed surface at 900 °C leading to the formation of a shallow defect. (b) Shows the agglomeration of eight tetraclusters at 950 °C to form a type B cluster of size ~14.3 Å and height ~2.3 Å. (c) The ordering of type B clusters at 1000 °C to form the (6×6) cluster phase on the 6H-SiC(0001) surface.

(14.3±0.5 Å) from STM. By preserving the integrity of a tetracluster unit (i.e., a size of ~8.0 Å and a height of ~1.5 Å) and using it as a basic building block, we were able to describe and account for type B clusters having a diameter of 14.3 Å and a height of 2.3 Å.[18] This would require an agglomeration of eight tetraclusters on the surface (seven tetraclusters in plane with the eighth on top[18]) which fits within the measured diameter, as shown in Fig. 5(b).

The phase transformation observed in this regime, i.e., $(3\times3)\rightarrow(6\times6)$ cluster phase therefore establishes the existence and identity of type A cluster. More significantly, it can also be used as a basic building block to account for the formation of larger type B clusters and the subsequent self assembly observed.[18]

2. **(6×6) clusters→(6×6)** *ring structure*

Figure 1(e) indicates that heating the (6×6) cluster surface to 1050 °C leads to disordering of the type B clusters and coexistence of other clusterlike features. However, upon annealing to higher temperatures at 1100 °C, the resulting surface topography [Fig. 1(f)] is surprisingly dominated by long-range ordering of ring structures instead. It is also interesting to note that the clusterlike features were no longer observed. This structural transformation is therefore studied in more detail by analyzing high-resolution STM snap shots of the surface as it is progressively heated to 1030, 1050, and 1100 °C, respectively.

Figure 6(a) (i) shows a 20 nm×20 nm STM image of the surface annealed to 1030 °C. The surface is now disordered and the inset image (4 nm×4 nm) shows the coexistence of two types of clusters with average sizes of ~8.0±0.5 Å and 14.3±0.5 Å, respectively. The cluster shape and dimensions measured from the line profile analysis in Fig. 6(a) (ii) are clearly identical to the type A and B clusters observed previously and are hence identified accordingly. In addition, these type A and B features appear to exist above a third underlying feature on the surface. This new feature is round in appearance and possesses an average size of ~3.0±0.5 Å. As they are observed for the first time during the experiment, we shall identify them as type C feature. At this temperature, the number of type A clusters and the C feature appears more than type B clusters. This is in contrast with the previous surface at 1000 °C, where type B clusters dominated [Fig. 1(d)].

When the surface is further annealed to 1050 °C, as shown in Fig. 6(b) (i) (20 nm×20 nm), the STM image shows that the occurrence of the type B clusters have diminished significantly. At this stage, only type A cluster appears remains and it appears to coexist with the ring structures which are detected for the first time. While the ring structures do not fully extend over the entire surface, it is interesting to note that the type A clusters are observed to sit preferentially on the corner sites of the ring structures which are aligned along the $[11\bar{2}0]$ and $[\bar{2}110]$ crystallographic azimuths. These type A clusters, consistent with earlier observation at 1030 °C, are again found to exist above the underlying type C feature on the surface. The high-resolution STM also shows that the rings are made up of a network of type C features and have a depression in the center as indicated in the inset picture.

The vertical line profile analysis indicated by *P* in Fig. 6(b) (ii) shows that the average height difference between a type A cluster and the neighboring ring depression is ~5.0±0.5 Å, while the vertical separation between type C feature and depth of the depression is ~2.0±0.5 Å as indicated by *Q*. The separation between type C features to the top of the type A cluster is thus ~3 Å. With the aid of Starke's (3×3) tetracluster model and structural dimensions, we can in fact account for the STM profile observed. The cross-sectional view of the ordered (6×6) cluster model is shown in Fig. 6(d) (i). Staggered removal of tetracluster units from the type B clusters as shown in Fig. 6(d) (ii) will result in a surface decorated by some type A clusters, type B clusters and in areas where tetraclusters are missing, underlying silicon adlayer will be exposed. This Si adlayer is the third layer of the original Starke structure and hence if we measured from the top of the type A cluster to the Si adlayer, a separation of 3 Å will be obtained (see Fig. 2).

By removing more Si atoms from the Si adlayer as well as tetraclusters from the remaining type B clusters from the structure as shown previously in Fig. 6(d) (ii), would generate a structure consisting of remnant type A clusters and underlying fourth and final Si layer atoms The resultant structure as shown in Fig. 6(d) (iii) would hence give rise to a depression of depth ~5.3 Å when compared against the peak of a neighboring type A cluster.

The STM line profile measurements therefore coincide with the values expected from the Starke model. The implication is that the type C features are associated with the Si-adlayer atom. Therefore, the disappearance of type B and the coexistence of type A, type C and holes on the surface would imply that apart from missing type A clusters, Si is also lost from the Si adlayer and most likely occurs from the region, where type A clusters are missing. At this stage, only Si atoms within the first three layers (tetracluster and adlayer) are removed in order to account for formation of type C feature and for the depth of the holes observed.

Figure 6(c) (i) shows the surface after it heated to 1100 °C. The density of type A clusters on the surface has reduced significantly and with the loss of these clusters, a network of ring structures now dominates the surface. The inset images show very clearly that the walls of each ring consisting of an individual C feature which we have attributed to be the Si originating from the third layer of the substrate. These type C feature appears to be linked together to form the wall of the ring structure which has a depression at the center. A closer study of the ring structure at 1100 °C reveals that the type C feature are arranged into either small trimerlike structures (termed D_1) or larger triangular features (termed D_2) which appear to alternate hexagonally to form the ring structure The high-resolution STM image [Fig. 1(c)] shows that D_1 consists of ~3 type C feature while the line profile analysis reveals that the mean separation between each type C feature is ~3.1±0.5 Å. The D_2 feature is observed to consist of ~10 type C feature which are uniformly arranged in an equilateral triangle-like structure with each side measuring to be ~9.0±0.5 Å. As the (1×1) unit cell of the bulk possesses a unit cell length of ~3.08 Å,[8] this unique formation of type C feature within both D_1 and D_2 indicates that the arrangement of type C feature follows the underlying registry of the bulk lattice site of the 6H-SiC(0001) substrate. We can therefore attribute this type C feature as an individual Si adatom.

STM vertical line profile as shown in Fig. 6(c) (ii), measuring from peak of D_1 and D_2 features to the holes of the ring shows that the average depth of a ring structure to be ~3.5±0.5 Å. Having identified that type C features on the surface are individual Si adatoms and that they were originally the third layer of the substrate, it is interesting to note that this measured depth is also comparable to the vertical separation measured from the third layer to the fifth layer of the Starke model for the (3×3) structure (see Fig. 2). At this stage, in the region where holes have developed, there is the

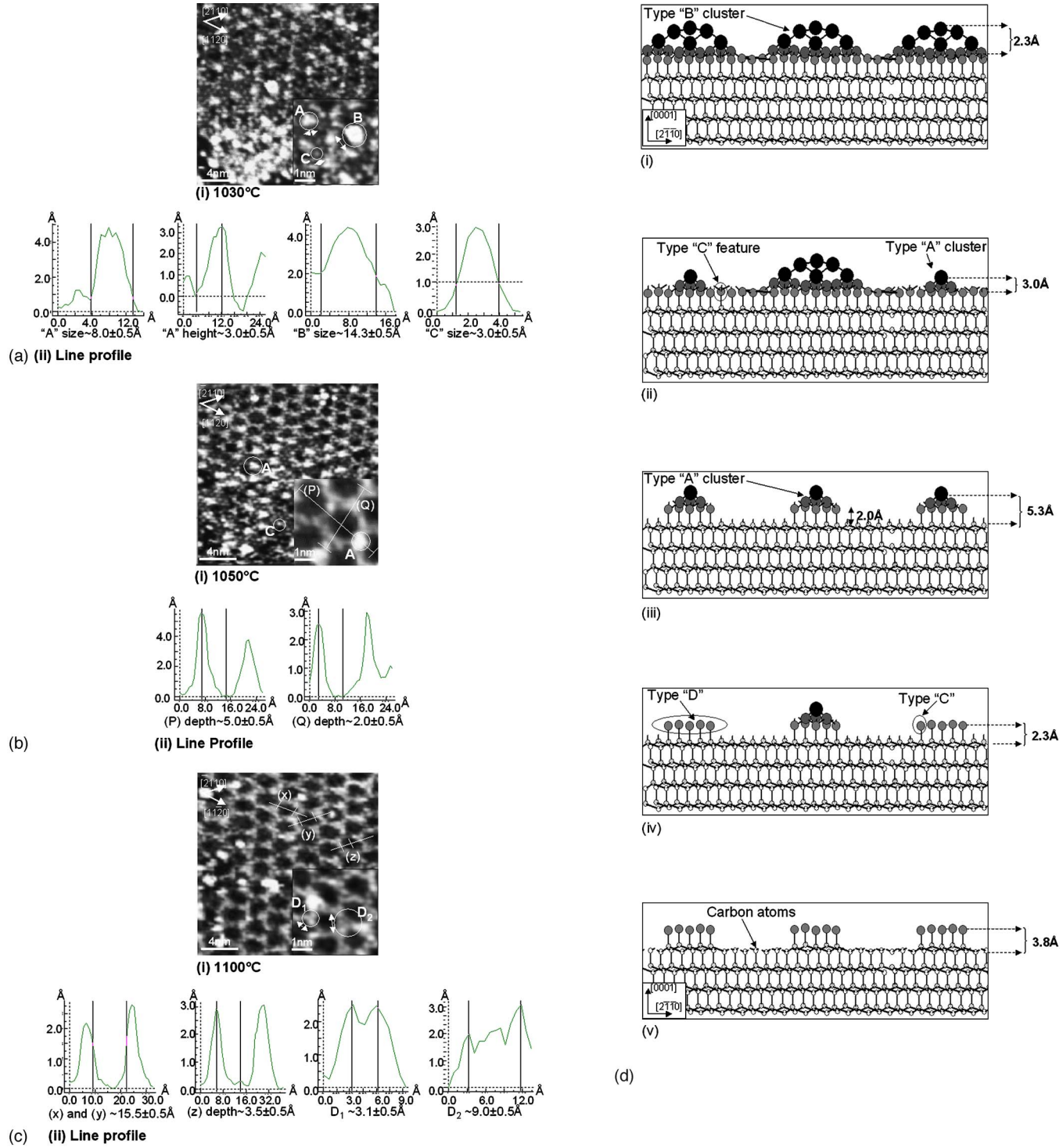

FIG. 6. (Color online) (a)–(c) (i) A 20 nm×20 nm STM image of the surface at 1030, 1050, and 1100 °C, respectively, with corresponding 4 nm×4 nm inset images. (a)–(c) (ii) Shows the line profile analysis of: a (ii) type A (size ~8.0±0.5 Å height ~3.0±0.5 Å), type B (size ~14.3±0.5 Å), and type C (size ~3.0±0.5 Å) features. (b) (ii) Respective depth profiles (*P*) ~5.0±0.5 Å and (*Q*) ~2.0±0.5 Å. (c) (ii) ring sizes (*x*) and (*y*) ~15.5±0.5 Å, ring depth ~3.5±0.5 Å, D_1 size ~3.1±0.5 Å, D_2 ~9.0±0.5 Å. (d) The schematic vertical profile of (i) (6×6) cluster phase at 1000 °C, (ii) formation of type A, B, and C features at 1030 °C, (iii) formation of type A clusters and shallow holes at 1050 °C, (iv) formation of type D features, and (v) formation of deep holes at 1100 °C.

absence of Si tetraclusters, a missing Si adlayer (third layer) and the underlying Si-terminated SiC bulk layer (fourth layer). The removal of these features from Fig. 6(d) (iv) will give rise to Fig. 6(d) (v). The depth of the depression measured with respect to the Si adatoms (third layer) will be ~3.8 Å which is again comparable to the measured line profile as shown in Fig. 6(c) (ii). Underlying C atoms will be exposed for the first time.

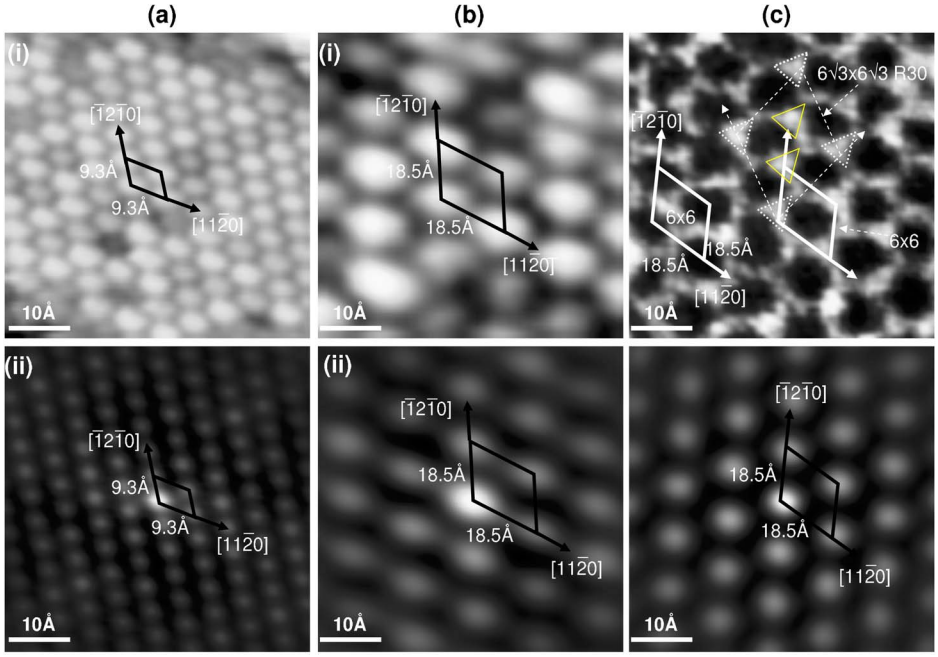

FIG. 7. (Color online) Real STM images (50 nm×50 nm) of (a) (3×3) reconstruction, (b) (6×6) clusters, and (c) (6×6) rings with respective unit cells illustrated. (c) (i) A dotted schematic representing a $(6\sqrt{3}\times 6\sqrt{3})R30°$ unit is superimposed on a (6×6) unit cell. (a)–(c) (ii) The corresponding self-correlated images with respective unit cells highlighted.

These STM observations shown in Fig. 6 therefore clearly indicate a loss of Si material from the substrate. The initial loss of Si from the surface destroys the (6×6) cluster periodicity and to the effect that it renders insufficient Si atoms on the surface to form the larger type B clusters. Instead, Si atoms exist primarily as type A clusters and also the emergence of type C Si adatoms. With further loss of Si from the surface, even the type A clusters are not seen and the surface is eventually dominated by type C Si adatoms which decorate the wall of the ring structure. The process first occurs with disappearance of type B clusters and then followed by type A clusters. The removal of tetraclusters would expose the Si adlayer and any missing Si adlayer atoms would expose the Si-terminated SiC bulk layer. Eventually the fifth layer which is a carbon layer will be exposed if more Si is lost. The progressive loss of Si and formation of holes on the surface is consistent with the trend of decreasing Si content demonstrated by the XPS data in Figs. 3 and 4. More importantly, the dominance of type C features and holes also meant that the loss of Si from the Si adlayer to form the holes most likely occurs from the region where type A clusters was originally missing. The details of this evolution will be discussed further in Sec. III C.

At present, it is interesting to note that these ring structures appears to have some periodic arrangement on the surface. The lateral line profile analysis of the ring structures indicate a uniform average separation of ~18.5±0.5 Å between the center of neighboring rings as shown by (ii) and (iii), in both [11$\bar{2}$0] and [$\bar{2}$110] directions as well as an average diameter of ~15.5±0.5 Å [indicated by (iv)]. Based on a (1×1) bulk unit cell length of ~3.08 Å,[8] this nearest-neighbor separation value would translate into a surface ordering with a periodicity 6 times that of the bulk. This observation differentiates the ring structure from the $(6\sqrt{3}\times 6\sqrt{3})R30°$. We will attempt to establish the periodic identity of the ring structure by comparing the unit cell dimensions of the (3×3) reconstruction, the (6×6) clusters and ring structures in real STM images with corresponding autocorrelated images.

Figure 7(a) (i) shows a 50 Å×50 Å STM real image of the (3×3) reconstruction obtained after annealing at 850 °C. The parallelogram illustrated on the image depicts a basic (3×3) unit cell indicating the two main crystallographic azimuths to be [$\bar{1}2\bar{1}0$] and [11$\bar{2}$0]. The average unit cell dimension in both directions is measured to be ~9.3 Å. Meanwhile, Fig. 7(a) (ii) is a corresponding autocorrelated image which shows similar (3×3) periodicity in the same [$\bar{1}2\bar{1}0$] and [11$\bar{2}$0] directions while the basic unit cell also displays identical dimensions of ~9.3 Å.

Figure 7(b) (i) is the STM real image (50 Å×50 Å) of the (6×6) ordered cluster arrangement. The parallelogram unit cell indicated on the image shows that the average cluster separations measure to be about ~18.5 Å giving rise to a (6×6) periodicity in the [$\bar{1}2\bar{1}0$] and [11$\bar{2}$0] azimuths. Figure 7(b) (ii) shown below is the extracted autocorrelated image, which shows that the unit cell derived does not defer from the real image in size or direction.

In Fig. 7(c) (i), the real STM image (50 Å×50 Å) of the surface shows the ring structures obtained at 1100 °C. Our STM line profile study shows that neighboring rings possess a uniform separation of ~18.5±0.5 Å, which translates into six times the periodicity for the observed surface structure with respect to the SiC(0001)-(1×1) unit cell. It is also important to note that the ring structures are also aligned in the [$\bar{1}2\bar{1}0$] and [11$\bar{2}$0] crystallographic azimuths with respect to the crystal bulk. We construct the resultant (6×6) unit cell in Fig. 7(c) (i) as indicated by the parallelogram in white bold lines with arrows indicating the [$\bar{1}2\bar{1}0$] and [11$\bar{2}$0] azimuths and each unit cell corner occupying the center of adjacent rings. A second (6×6) unit cell is constructed with each corner sitting on neighboring bright features to show that the

entire ring structure adheres to the (6×6) periodicity.

The autocorrelated image in Fig. 7(c) (ii) indicates a unit cell following the $[\bar{1}2\bar{1}0]$ and $[11\bar{2}0]$ directions with identical dimensions of ~18.5 Å dominating the real STM image. The existence of a $(6\sqrt{3}\times6\sqrt{3})R30°$ structure would produce a pattern with unit cell dimensions of ~32 Å with an angular difference of 30° from the $[\bar{1}2\bar{1}0]$ and $[11\bar{2}0]$ azimuths. However, this structure is absent from the self-correlated image, hence we can rule out the existence of a $(6\sqrt{3}\times6\sqrt{3})R30°$ structure from the real space STM images.

In order to resolve the possible existence of a $(6\sqrt{3}\times6\sqrt{3})R30°$ structure as seen in LEED experiments,[17] we superimpose a $(6\sqrt{3}\times6\sqrt{3})R30°$ white dotted unit cell on the second (6×6) unit cell. It is also clear from the comparison that the basic ring structure does not subscribe to the $(6\sqrt{3}\times6\sqrt{3})R30°$ unit cell, while the (6×6) unit cell provides a good description for the ordering shown in the real image. To account for the existence of the $(6\sqrt{3}\times6\sqrt{3})R30°$ reconstruction, the structure would have to coincide with the bright features outlined in dotted triangles in Fig. 7(c) (i). However, it would be necessary to selectively remove the bright features marked by the bold triangles, to allow the remaining features to exist as dominant scattering centers in order to obtain the $(6\sqrt{3}\times6\sqrt{3})R30°$ unit cell.

The autocorrelation analysis therefore also lends support to the XPS and STM study. The ring structure obtained at 1100 °C therefore follows a (6×6) periodic arrangement and it does not possess a $(6\sqrt{3}\times6\sqrt{3})R30°$ unit cell. In fact, XPS data shows that this super structure is still Si rich, albeit less Si rich compared to the (6×6) cluster and the initial (3×3) surface. It is also not the (6×6) trimer structure as seen by Owman *et al.*[16] Corelating the surface morphology observed by STM with the XPS data would imply that the mechanism responsible for the surface restructuring occurs in the presence of clusters, depressions and holes, and loss of Si from the surface. Specifically, the STM data obtained from the transformation of (3×3) to (6×6) clusters have shown that Si adatoms prefer to exist as type A clusters when "popping" out from the (3×3) phase during annealing. The evidence of type A clusters reemerging during the surface evolution from the (6×6) clusters to the (6×6) ring structures appear to suggest that this process may again be facilitated by type A Si tetraclusters. The implication is the involvement of these Si tetraclusters in facilitating the phase transformation, Si-material loss, and the subsequent atomic restructuring of the surface to form the ring structure.

Motivated by the above observations, we will attempt to propose a mechanism, taking into consideration the role of Si atoms in the form of $M\times$Si tetraclusters (where M is the number of clusters) as a building block, to describe the structural transformation observed. As we have already shown that $8\times$Si tetraclusters are involved in the formation of the (6×6)-cluster phase,[18] we will only describe how the formation of the ring structure and the occurrence of type A, B, C, D_1, and D_2 features develop as we heat the SiC(0001)-(6×6) surface from 1000 to 1100 °C in the next section. We will show that by selectively moving $M\times4$ units from the structural models at each respective annealing temperature, we will be able to account for the basic morphological features observed in this regime and hence deduce the minimum number of Si atoms required to reproduce the basic structural framework of a ring feature and its (6×6) periodicity on the SiC surface.

C. Structural model for cluster mediated formation of (6×6) rings

In order to form the final (6×6) ring structure, we will need to remove at least a total of $M=19$ Si tetraclusters (76 Si atoms) per unit cell from the initial (6×6) cluster structure. The process by which this occurs is shown schematically in Figs. 8–10. The ball and stick models presented are closely based on the STM data in terms of physical dimensions measured and the structural evolution observed as the surface is annealed from 1000 to 1100 °C.

When the surface is annealed to 1030 °C, disordering of the (6×6) cluster phase takes place while the formation type A, B, and C features are observed [Fig. 6(a) (i)]. In order to account for this observation, we remove $M=7$ tetraclusters per unit cell in a staggered manner from the original (6×6) cluster arrangement [Fig. 8(a)]. In doing so, we obtain the schematic diagram in Fig. 8(b) which depicts a surface morphology consisting of residual type B clusters and a majority of type A clusters and C features which we have identified as the Si adlayer atoms (i.e., third layer Si adlayer of the Starke model). In fact, the reduction in area coverage of the type B clusters also exposes the underlying type C features which is synonymous with the STM observation in Fig. 6(a) (i). The complete removal of the $M=7$ tetraclusters from each unit cell would result in a unit cell consisting of $M=1$ tetracluster and the Si adlayer (type C feature) as shown in either Figs. 8(c) or 8(d). We note that this structure has not been observed experimentally. Instead, the STM data obtained at 1050 °C shows formation of a shallow ring structure with a hole in the center coexisting with type A clusters and type C feature. The size of the hole is $\sim15.5\pm0.5$ Å and depth is $\sim5.0\pm0.5$ Å [Fig. 6(c) (i)]. In order to account for this ring size, we will need to remove from Fig. 8(c) or Fig. 8(d) another 20 Si atoms or $M=5$ tetracluters.

However, we can generate this shallow ring structure by removing the Si atoms from either two hexagonal regions between the type A clusters, as shown in Fig. 8(c) and 8(d) respectively. Hence, at this stage we will introduce two possible routes by which loss of Si atoms from the surface occurs. We will show that the two pathways will in fact lead to the formation of an identical (6×6) ring structure and also involves the same number of tetraclusters.

1. Loss of Si via pathway 1

The loss of Si atoms via the first route would require removing 20 Si atoms which are highlighted as shown in Fig. 8(c). This would generate a shallow ringlike structure with a diameter of ~15.5 Å and a depth of ~5.3 Å. The removal of these 20 Si atoms will also expose the underlying Si atoms (i.e., fourth layer Si atoms of the Starke model) and they will also be bordered by the remaining Si atoms of the original

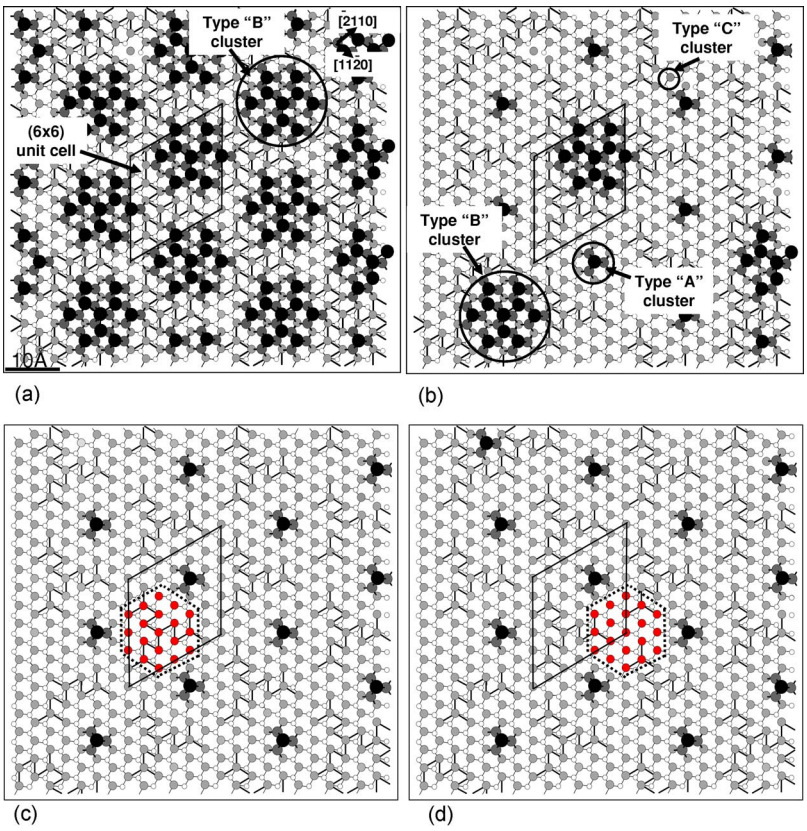

FIG. 8. (Color online) A plane view of the ball and stick model illustrating the surface structural evolution as a function of temperature. (a) (i) The (6×6) cluster phase consisting of type B clusters at 1000 °C. (ii) The staggered removal of $M=7$ tetraclusters per unit cell from the surface in (i), leading to the formation of a surface consisting of type A, B, and C features, corresponding to STM images at 1030 °C. (iii), (iv) The surface after the complete removal of $M=7$ clusters. Two regions from which 20 Si atoms are removed to generate the shallow ring structure as highlighted, respectively, in (iii) and (iv).

third layer. In doing so, preferential sitting of the type A clusters at the corner sites of each ring structure will also be observed. This ring structure with a shallow depression is indicated by the dotted hexagon as shown in Fig. 9(a). The resulting structure is consistent with the surface topography as imaged by the STM shown previously in Fig. 6(b) (i).

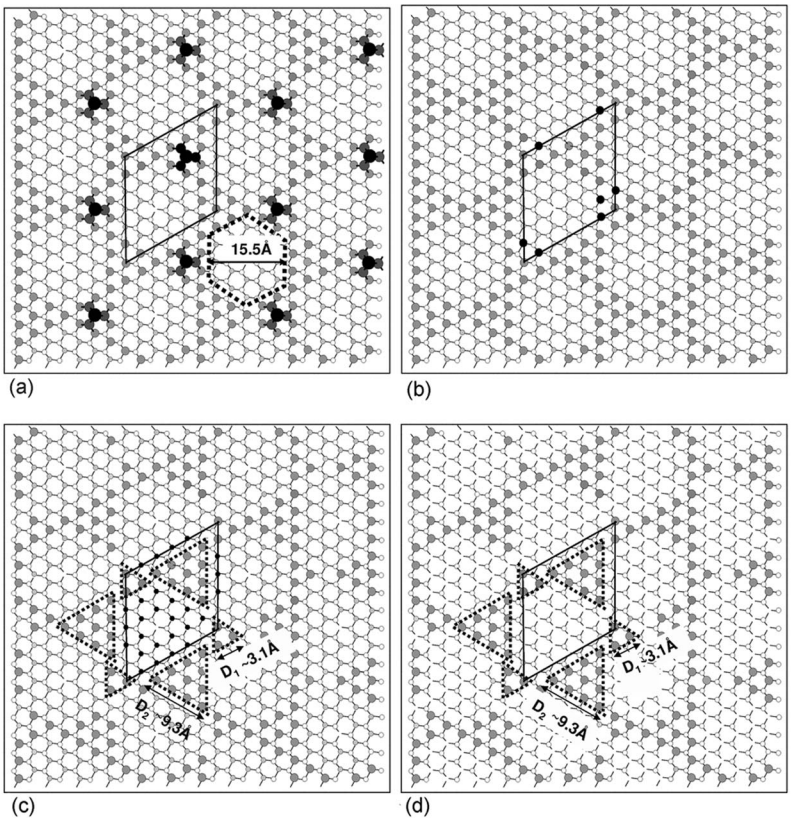

FIG. 9. (a)–(d) describe the progressive removal of $M\times4$ clusters per unit cell to obtain the final (6×6) ring structure through pathway 1. (a) The surface after removal of 20 atoms $(M=5)$ highlighted previously in Fig. 8(c). These atoms were removed from the third and fourth layer of the U. Starke structure to generate the resultant shallow ring structure with ring size ~15.5 Å at 1050 °C. (b) The remaining type A clusters which exist at the corner sites as shown in (a) is removed $(M=1)$ to account for their absence in the STM images. The remaining third layer atoms form the resulting boundary of the ring structure. (c) Four atoms $(M=1)$ within this layer as highlighted in (b) were removed to account for the measured triangular $D_1\sim3.1$ Å and $D_2\sim9.3$ Å sizes. (d) 20 Si atoms $(M=5)$ are removed from the fourth layer as indicated in (c) to account for the final ring structure and the whole process therefore involves $M=19$ clusters in total.

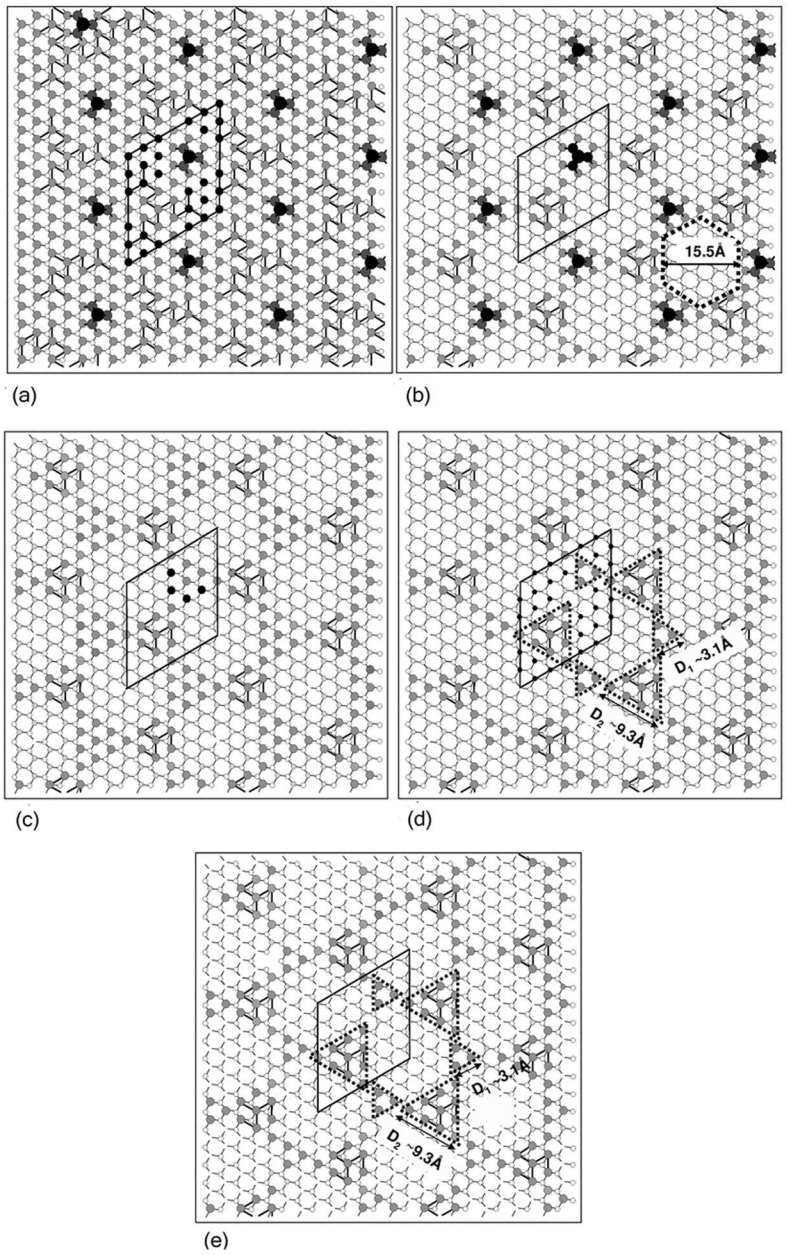

FIG. 10. (a)–(e) describe the progressive removal of $M\times4$ clusters per unit cell to obtain the final (6×6) ring structure through pathway 2. (a) shows the alternative region, as indicated by the 20 highlighted Si atoms ($M=5$) which are removed to form (b). The highlighted type A clusters as shown in (b) is removed ($M=1$) to account for their absence in the STM images. The resulting ring structure as shown in (c) is indicated by the boundary formed by the third layer atoms. There are four atoms highlighted within this layer which are removed ($M=1$) to account for the measured triangular $D_1\sim3.1$ Å and D_2 ~9.3 Å sizes as shown in (d). The removal of 20 Si atoms ($M=5$) from the fourth layer as highlighted in (d) accounts for the deep holes observed and this results in the final ring structure as shown in (e). The whole process again involves $M=19$ clusters in total.

Proceeding further, we will need to account for the prevalent existence of type C Si atoms which form the D_1 and D_2 triangular features. These features are in turn arranged into ordered networks which generate the resultant (6×6) ring structure as observed at 1100 °C. In order to describe these structural characteristics, we will need to remove another 28 Si atoms ($M=7$) from the unit cell. The following Si atoms are removed, (1) Four Si atoms ($M=1$) i.e., type A cluster which existed at the corner sites as shown in Fig. 9(a) is removed. This would give rise to the surface structure shown in Fig. 9(b), which is consistent with the absence of the type A clusters in the STM data at this stage, (2) In order to account for the observation of D_1 and D_2 features, we selectively remove four Si atoms per unit cell from Si atoms from the third and fourth layer ($M=1$) as indicated in Fig. 9(b). In doing so, the remaining third layer Si adatoms would form the boundary of the ring structure shown in Fig. 9(c). By following registry of the SiC (1×1) structure, the arrangement of remaining Si adlayer adatoms would form equilateral triangular structures of two sizes with side lengths measuring ~3.08 and ~9.3 Å, respectively, as outlined by dotted triangles in Fig. 9(c). These dimensions match closely with the measured lengths of the D_1 (size $\sim3.1\pm0.5$ Å) and D_2 (size $\sim9.0\pm0.5$ Å) triangular features in the STM scans. By arranging these two features in an alternating hexagonal structure, would result in a hexagonal ring structure with an average uniform diameter of ~15.5 Å that follows the (6×6) periodicity, (3) Finally, to account for the vertical profile analysis earlier in Fig. 6(c) (iii), we will need to remove another 20 Si atoms ($M=5$) from the exposed fourth layer of Si atoms as indicated in Fig. 9(c). This would give a ring structure as shown in Fig. 9(d) with a depth of $\sim3.5\pm0.5$ Å measured against the peak of D_1 and D_2 features. A total of 19 tetraclusters is thus involved.

2. Loss of Si via pathway 2

In the second route, we selectively remove 20 Si atoms ($M=5$) from the third layer which are highlighted in the unit cell as shown in Fig. 10(a) [these atoms are equivalent to those highlighted in Fig. 8(d)]. By releasing these atoms highlighted in Fig. 10(a), from each unit cell, we will again obtain a shallow ring structure of size ~15.5 Å and depth ~5.3 Å while exposing the fourth layer Si atoms. The resulting ring structure shown in Fig. 10(b) will consist of the remaining Si adlayer atoms from the original third layer as well as type A clusters which sits at the corner of the ring corresponds closely to the STM image of the surface observed at 1050 °C.

Similar to earlier discussion, we will need to account for the absence of type A clusters, the prevalent existence of type C Si atoms which forms D_1 and D_2 triangular features and the resultant (6×6) ring structure which is observed at 1100 °C. To describe these features, we again need to remove another 28 Si atoms ($M=7$) from this unit cell. The absence of type A clusters at 1100 °C, means we need to remove one type A cluster ($M=1$) from each unit cell as shown in Fig. 10(b), to generate the resultant surface shown in Fig. 10(c). However, the presence of the D_1 (size ~3.1±0.5 Å) and D_2 (size ~9.0±0.5 Å) features observed by STM further dictates the removal of four Si atoms ($M=1$(from the third and fourth layer from each unit cell as highlighted in Fig. 10(c). Consequently, the surface structure shown in Fig. 10(d) will now consist of smaller triangular features (size ~3.08 Å) and larger triangular features (size ~9.3 Å) consisting of coplanarly bonded Si atoms, which correspond to the observed D_1 and D_2 features respectively. As the STM line profile analysis have demonstrated a ring depth of ~3.5±0.5 Å stemming from the loss of Si from the fourth layer, hence we will need to remove the remaining 20 atoms or $M=5$ tetraclusters from the exposed fourth layer Si atoms as indicated in Fig. 10(d). This would generate a ring structure of respective depth ~3.8 Å and size ~15.5 Å with triangular D_1 and D_2 features [Fig. 10(e)] which accounts for the STM image analysis. The final ring structure obtained here is the same as the one obtained through pathway 1 and again involves a total of 19 tetraclusters.

Given the present experimental results, we are not able to resolve the dominating pathway. Nevertheless, it is clear that irrespective of the route in which Si may be loss, the same number of Si atoms equivalent to $M=19$ tetraclusters were removed from the initial (6×6) cluster phase to obtain the final ring structure shown in Fig. 9(d) or Fig. 10(e). In addition, the resulting ring structure which is formed also involves the removal of Si atoms from the original fourth layer Si atoms of the Starke's model. Hence underlying top layer of C atoms of the SiC bulk would also be exposed for the first time at this stage. This would result in greater Si-C bonding as detected by XPS, which indicates a more intense Si-C signal as compared to the Si-Si at this temperature. In principle, formation of C-C bonds within the hole may result since it will reduce the number of carbon dangling bonds. We were not able to image these carbon atoms within the holes. However, it is interestingly to note at this stage, the C 1*s* peak is still dominated by the Si-C chemical environment. The shift in binding energy to 285 eV only occurs later at 1200 °C where a graphitic surface has been reported[13,14] to dominate the SiC surface. This would imply further loss of Si atoms from the fourth layer leading to the eventual formation of a carbon rich surface.

We have shown that by selectively moving $M\times4$ units from the structural models at each respective annealing temperature, we are able to account for the basic morphological features observed and also deduce the minimum number of Si atoms required to reproduce the basic structural framework of a ring feature and its (6×6) periodicity on the SiC surface. By defining a unit volume as a (6×6) unit cell area consisting of the top four layers where Si-Si bonding dominates, the (3×3) structure would consist of 88 Si atoms per unit volume. It is clear from the structural evolution illustrated by the two pathways in Figs. 9 and 10, a removal of at least $M=15$ clusters or 60 atoms per unit volume from the initial (3×3) reconstruction is therefore necessary to obtain a (6×6) ring structure which describe the STM data.

In order to ascertain if this proposed ball and stick model agrees with stoichiometric information from XPS, we compare the loss of 60 Si atoms derived from the model with that deduced from comparing the XPS intensity obtained for elemental Si at 850 °C [$(I_{(3\times3)})$, where ordered (3×3) reconstruction is observed] and that at 1100 °C [$(I_{(6\times6)\ \mathrm{rings}})$, where ordered (6×6) ring structure is observed].

The peak area intensity for the elemental Si $2p$ XPS peak is related to the atomic concentration of Si atoms per unit volume (N_{Si}) by the following expression:

$$I_{\mathrm{Si}} = N_{\mathrm{Si}} \times \mathrm{ASF} \times \mathrm{TF},$$

where I_{Si} is the peak area of Si $2p$ for Si-Si, ASF is the atomic sensitivity factor, and TF is the transmission function. Since ASF and TF are constants for the same element, we are able to compare the XPS intensity (I) with atomic concentration of atoms per unit volume (N) for both (3×3) and (6×6) rings in the following expression:

$$\frac{I_{(3\times3)}}{I_{(6\times6)\ \mathrm{rings}}} = \frac{N_{(3\times3)}}{N_{(6\times6)\ \mathrm{rings}}}.$$

In the current experiment, $I_{(3\times3)}$ has a value of 726 counts. This is associated with the (3×3) structure consisting of 88 Si atoms per unit volume as previously defined ($N_{(3\times3)}=88$). With the value of the XPS peak area intensity for the (6×6) ring structure ($I_{(6\times6)\ \mathrm{rings}}$) equal to 236 counts, we can therefore estimate the value of $N_{(6\times6)\ \mathrm{rings}}$ from the above expression to be 28. This value is equivalent to the number of Si atoms found within the model describing the (6×6) ring structure. Consequently, the difference in the number concentration of Si per unit volume between the two phases is 60. Hence, quantitative analysis of the XPS data not only shows a clear loss of Si with annealing resulting in increased exposure of the SiC bulk, but also agrees with the proposed model of Si loss via selective removal of M tetraclusters.

The progressive loss of Si in terms of $M\times4$ Si atom units will also be consistent with two other key experimental ob-

servations of tetraclusters during the phase transformation of the 6H-SiC(0001)-(3×3) surface to (6×6) ring structure, (1) The observation of type A clusters being released from the (3×3) reconstruction. This suggest a natural tendency for Si adatoms to come together to form a Si_4 cluster, (2) The agglomeration Si_4 clusters to form the new (6×6) cluster phase,[19] the formation of same sized type A clusters after the disappearance of type B clusters due to heating and the eventual formation of the ring structure also suggest that this unique cluster is an important vehicle for Si mass transport in facilitating the surface structural transformation. These experimental observations point towards the existence of type A cluster as a unique stable structure for Si atoms on the SiC(0001) surface. This is surprising given that the Si atoms within the cluster are likely to possess nonideal tetrahedral bonding unlike that of Si atoms in the bulk. Recently, Grass *et al.*[20] reported the existence of Si magic clusters consisting of four Si atoms on HOPG. The Si_4 clusters, however, were deposited from a cluster source, and together with theoretical calculations showed that these clusters are stable against coalescence at room temperature. It will thus be of an interest to study these magic clusters from a theoretical approach and hence derive a minimum energy structure to rationalize their existence on the SiC(0001) surface.

IV. CONCLUSION

In this work, we study the formation of (6×6) rings using STM and XPS as a function of temperature. While the XPS shows that the ring surface is still Si rich and not yet graphitized, the analysis of the STM data with line profile measurement and autocorrelation in studying the periodicity and alignment shows that the rings are arranged in a (6×6) periodicity with an absence of the $(6\sqrt{3}\times6\sqrt{3})$ $R30°$ reconstruction. High-resolution STM images show the formation of type A clusters from type B leading to the ring structure formation made up of type C Si adatoms when the surface is heated beyond 1000 °C. The presence of type A clusters participating in the phase transformation suggests that the magic number of four Si atoms is a stable structure and is also important in mediating the surface structural transformation. Using XPS and STM data which show loss of Si with progressive annealing, we propose a model to illustrate this surface evolution through the selective removal of $M\times4$ Si atoms (where M is the number of clusters) at various annealing temperatures. With this proposed mechanism, we remove $M=19$ pre unit cell to obtain model of a ring structure consisting of locally organized type C Si adatoms arranged into hexagonal D_1 and D_2 formations, which are in good agreement with the experimental data. It should be noted that this is the minimum number of atoms needed to account for the formation of rings. More material can clearly be removed and this will account for irregularity of ring walls.

ACKNOWLEDGMENTS

We thank Drs. H. Xu, X. N. Xie, K. P. Loh, A. C. H. Huan, and A. T. S. Wee for help with the initial substrate cleaning and sample preparation. We gratefully acknowledge the financial support from NUS and IMRE under the Atomic Layer Epitaxy Programme.

*Corresponding author. Electronic address: phytokes@nus.edu.sg

[1] A. K. Agarwal, S. Seshadri, M. Macmillan, S. M. Sita, J. Casady, P. Sanger, and P. Shah, Surf. Sci. Spectra **44**, 303 (2000).
[2] G. L. Harris, *EMIS Data-Reviews Series* No. 13 (IEEE, London, UK, 1995).
[3] V. van Elsbergen, T. U. Kampen, and W. Monch, Surf. Sci. **365**, 443 (1996).
[4] T. Tsukamoto, M. Hirai, M. Kusaka, M. Iwami, T. Ozawa, T. Nagamura, and T. Nakata, Surf. Sci. **371**, 316 (1997).
[5] M. Naitoh, J. Takami, S. Nishigaki, and N. Toyama, Appl. Phys. Lett. **75**, 650 (1999).
[6] I. Forbeaux, J-M. Themlin, V. Langlais, L. M. Yu, H. Belkhir, and J-M. Debever, Surf. Rev. Lett. **5**, 193 (1998).
[7] U. Starke, J. Schardt, and M. Franke, Appl. Phys. A: Mater. Sci. Process. **65**, 587 (1997).
[8] U. Starke, J. Schardt, J. Bernhardt, M. Franke, K. Reuter, H. Wedler, K. Heinz, J. Furthmuller, P. Kackell, and F. Bechstedt, Phys. Rev. Lett. **80**, 758 (1998).
[9] J. Schardt, J. Bernhardt, U. Starke, and K. Heinz, Phys. Rev. B **62**, 10335 (2000).
[10] K. Heinz, U. Starke, J. Bernhardt, and J. Schardt, Appl. Surf. Sci. **162**, 9 (2000).
[11] J. E. Northrup and J. Neugebauer, Phys. Rev. B **52**, R17001 (1995).
[12] L. I. Johansson, F. Owman, and P. Martensson, Phys. Rev. B **53**, 13793 (1996).
[13] M. H. Tsai, C. S. Chang, J. D. Dow, and I. S. T. Tsong, Phys. Rev. B **45**, 1327 (1992).
[14] L. Li and I. S. T. Tsong, Surf. Sci. **351**, 141 (1996).
[15] L. I. Jonhansson, F. Owman, and P. Martesson, Phys. Rev. B **53**, 13793 (1996).
[16] F. Owman and P. Martensson, Surf. Sci. **330**, L639 (1995).
[17] W. Chen, K. P. Loh, H. Xu, and A. T. S. Wee, Appl. Phys. Lett. **84**, 281 (2004).
[18] E. S. Tok, W. J. Ong, H. Xu, and A. T. S. Wee, Surf. Sci. **558**, 145 (2004).
[19] W. J. Ong, E. S. Tok, H. Xu, and A. T. S. Wee, Appl. Phys. Lett. **80**, 3406 (2002).
[20] M. Grass, D. Fischer, M. Mathes, G. Gantefor, and P. Nielaba, Appl. Phys. Lett. **81**, 3810 (2002).
[21] A. Catellani, G. Galli, and F. Gygi, Phys. Rev. Lett. **77**, 5090 (1996).